Journal of Nuclear Materials 390–391 (2009) 227–231

Contents lists available at ScienceDirect

Journal of Nuclear Materials

journal homepage: www.elsevier.com/locate/jnucmat

Carbon transport in the stochastic magnetic boundary of TEXTOR

G. Telesca [a,*], E. Delabie [b], O. Schmitz [a], S. Brezinsek [a], K.H. Finken [a], M. von Hellermann [b], M. Jakubowski [c], M. Lehnen [a], Y. Liang [a], A. Pospieszczyk [a], U. Samm [a], M. Tokar [a], B. Unterberg [a], G. Van Oost [d], The TEXTOR Team

[a] Institut für Energieforschung - Plasmaphysik, Forschungszentrum Juelich GmbH, Association EURATOM-FZJ, Trilateral Euregio Cluster, Jülich, Germany
[b] FOM-Institute for Plasma Physics Rijnhuizen, Association EURATOM-FOM, Trilateral Euregio Cluster, The Netherlands[1]
[c] Max-Planck-Institut fuer Plasmaphysik, IPP-EURATOM Association, Teilinstitut Greifswald, Wendelsteinstr. 1, Germany
[d] Department of Applied Physics, Ghent University, Plateaustr. 22, B-9000 Gent, Belgium

ARTICLE INFO

PACS:
52.25.Fi
52.25.Vy
52.55.Fa

ABSTRACT

For given conditions, significant change in main particle and carbon transport is observed in TEXTOR under the action of the Dynamic Ergodic Divertor, DED, operating both in 6/2 and 3/1 basic modes. In particular, the stochastic layer created at the plasma edge by the applied perturbing field, is responsible for the so called pump out, PO, effect (observed in DIII-D and on JET during experiments of ELM mitigation) characterized by a decrease in the plasma density and the reduction in the intrinsic carbon concentration in the plasma core. For a sufficiently high value of the applied field strength, in DED 3/1 basic operational mode a 3/1 island connects to the wall, with related further enhancement of particle transport. With respect to carbon, this phenomenon simply leads to a further carbon de-contamination from the central plasma.

1. Introduction

In magnetic confinement experiments, external perturbing fields are used since long for mode control and for improving the power exhaust through enhanced transport and radiation at the plasma edge. More recently, it has been shown on DIII-D [1] and on JET [2] that the application of Resonant Magnetic Perturbations, RMP, may result in the mitigation of the Edge Localized Modes (ELMs). RMP lead to near-field effects and to the formation of chains of magnetic islands which may overlap, resulting in a strong modification of the original magnetic structure. The topology of the perturbed structure, which is generally composed by a zone of short connection length at the plasma periphery (the so called laminar zone) and by islands surrounded by a sea of stochastic field [3], depends on the strength of the applied field, on the poloidal (m) and toroidal (n) modes of the RMP and on the parameters of the target plasma. In this work we describe the experimental facts related to the change in particle transport, and more specifically in carbon transport, as derived from the data analysis of a large variety of TEXTOR discharges under the action of the Dynamic Ergodic Divertor, DED [4]. In the following, 'boundary plasma' means that part of the plasma volume outside the normalized poloidal flux tube $\psi_N = 0.8$ (i.e. $\psi_N > 0.8$) and 'central plasma' the plasma center, near the magnetic axis.

The three operational basic modes of DED (m/n = 12/4, 6/2 and 3/1) differ in their spectra and in their field penetration, causing different modifications of the magnetic structure at the plasma edge. In fact, the radial power-law dependence (the field penetration) of the perturbing field is, for linear approximation, $B_r \sim (r/r_{DED})^{\gamma}$ where r_{DED} is the radial position of the coils (in TEXTOR r_{DED} = 0.53 m) and γ = 19, 9 and 4 for the basic modes m/n = 12/4, 6/2 and 3/1, respectively, see Ref. [4]. These values have been calculated-for each n-considering the dependence of γ on the DED spectrum of the poloidal m modes and on the plasma parameters, as the pitch angle of the field lines and the plasma energy. The resulting radial extension of the perturbed zone increases with decreasing the toroidal n number while the magnetic structure of the stochastic layer depends also on the strength of the applied perturbing field, i.e. on I_{DED}. For the basic mode m/n = 3/1, the perturbing field reaches the 2/1 rational surface and, for a sufficiently large current in the DED coils (I_{DED}), the m/n = 2/1 tearing mode can be triggered. (It is worth mentioning that for standard TEXTOR plasma operation, without DED, m/n = 2/1 as well as m/n = 3/1 tearing mode is not observed, with the exception of some discharges with injection of high Z impurities.) Although the influence of the m/n = 12/4 basic mode on the magnetic topology is well documented by the formation of the helical divertor structure [5,6], its impact on main particle and impurity carbon transport is

* Corresponding author. Tel.: +49 2461 615174.
E-mail address: g.telesca@fz-juelich.de (G. Telesca).
[1] www.rijnh.nl.

0022-3115/$ - see front matter © 2009 Elsevier B.V. All rights reserved.
doi:10.1016/j.jnucmat.2009.01.061

marginal due to its very low penetration depth. In the following, we will focus on the implications for carbon transport of the application of DED in the basic modes $m/n = 6/2$ and 3/1.

Changing the conditions, the application of DED can lead to opposite effects in relation to particle transport, causing increase or decrease in particle and impurity confinement [7]. We limit the present analysis to situations with reduced particle confinement for two reasons. First, we are primarily interested in scenarios with lower impurity content and, second, the reduction of the pedestal density, the so called particle pump out, PO, is an important ingredient for ELM mitigation at DIII-D and JET [1,2] in low collisionality plasmas.

2. Experiments

Preliminary studies [8,9] on the change in carbon transport with DED have shown, both for 6/2 and 3/1 DED basic operational modes, enhanced screening and decrease of carbon concentration in the plasma center. However, these studies refer to TEXTOR discharges in which DED triggers 2/1 tearing mode activity for 3/1 DED basic mode and 3/1 tearing for 6/2 DED basic mode. In contrast, for the discharges considered here, tearing activity is absent or at a marginal level, thanks to the injection of significant Neutral Beam Counter (NBI-Cnt) power. Indeed, in the meanwhile it has become clear that injection of Neutral Beam Counter shifts towards higher values of I_{DED} the threshold for tearing modes, triggered by DED [10]. A second aspect which distinguishes the present work from preliminary studies is the use of an upgraded carbon diagnostic described in the next Section 2.1.

2.1. Diagnostics

The main diagnostic tool used in this study is a spectroscopic system by which a CIII (229.6 nm, upper level at 18 eV) and a CV (227.1 nm, upper level at 304 eV) line intensities are measured simultaneously, at 20 kHz sampling rate, along the nine lines of sight (1–9) depicted in Fig. 1. Five channels (*N*. 5–9) intercept the graphite divertor plates in the High Field Side, HFS, where the DED coils are located while the other four (*N*. 1–4) provide information on carbon behaviour relatively far from the target plate. Additionally, the CIII line is measured on one channel (*N*. 10) pointing at the graphite belt toroidal ALT-II limiter in the Low Field Side, LFS. Since the optical system is anchored to the tokamak vessel, the actual lines-of-sight of the 10 channels during the experiments-with vessel at temperature in excess of 200 °C-might slightly differ from those depicted in Fig. 1, which are derived from in situ inspection at room temperature. Fig 1 shows also the vacuum approximation of the magnetic field topology for the 3/1 basic mode. Different colors refer to different connection lengths: long connections define the stochastic region while the short ones define the laminar zone [6,7]. Even though the actual lines of sight may slightly differ from those depicted in the figure, from Fig. 1 one can notice that channels 9–8 point to the vicinity of the strike points as here the target is magnetically connected to the deep interior of the plasma by very long connection length while channels 6–5 point to the private flux region (defined as the region with very short connection length, $L_C < 10$ m). It is worth mentioning that the vacuum approximation of Fig. 1, which does not affect the actual position of the strike points as well as that of the private region, shows good agreement between reconstructed magnetic topology and measured edge parameters as the heat flux patterns, and it has been validated in the plasma edge ($\psi_N > 0.8$) for low rotation and for L-mode plasmas [3,11]. The intensity of CIII line is often taken as an indication for the level of the carbon flux (see Ref. [8]) because of the low ionization potential of the Be-like C^{2+} ions (48 eV) and it is also nearly proportional to the total radiated power, since carbon is the main intrinsic impurity in TEXTOR. On the other hand, the CV line intensity (ionization potential of C^{4+} ions = 392 eV) is instead related to the carbon density in the confined plasma.

The C^{6+} ion concentration in the plasma center is measured with the Charge Exchange Recombination Spectroscopy, CXRS, and the local electron density and temperature profiles at the plasma edge are measured on the LFS with the He-beam diagnostic [12] at the same toroidal sector where the CIII/CV diagnostic is located. With respect to the errors in the measurements shown in the figures of this paper, the following points have to be made:

(1) The time traces of CIII and CV line intensities as shown in Figs. 2 and 4 are simply non-calibrated signals, in arbitrary units.
(2) We show in Figs. 2 and 4 the data points of the local measurements of T_e and n_e; the standard deviation of the smooth time traces is about 10% for T_e and about 20% for n_e (please see Ref. [12] for a detailed discussion on the accuracy of the He-beam diagnostic). The T_e and n_e measurements in Fig 2 refer to the last close flux surface ($r = 0.46$ m) while those in Fig. 4 refer to 2 cm inside the scrape-off-layer ($r = 0.48$ m).
(3) The ratios, reported in Figs. 3 and 5, are calculated by averaging the CIII and CV spectroscopic signals over 200 ms during the flat top phase of DED, where the signals are practically constant in time. Considering the 20 kHz sampling rate of the spectroscopic signals and the long integration time, the 95% confidence interval of the value of the signals is very small (few millivolts) resulting in the error of their ratios on the order of a few percent.
(4) The small error bar shown in the time traces of Fig. 6 is the statistical error on the fit (i.e. on the extraction of the active charge exchange component from the spectrum) while the large one is the total absolute error on the carbon concentration which includes an assumption of 10% error on the product of the electron density with the beam stopping cross-section For the practical point of view, the level of the relative error in the carbon concentration (the one we are interested in when comparing the carbon concentration) is in between the statistical and the absolute one.

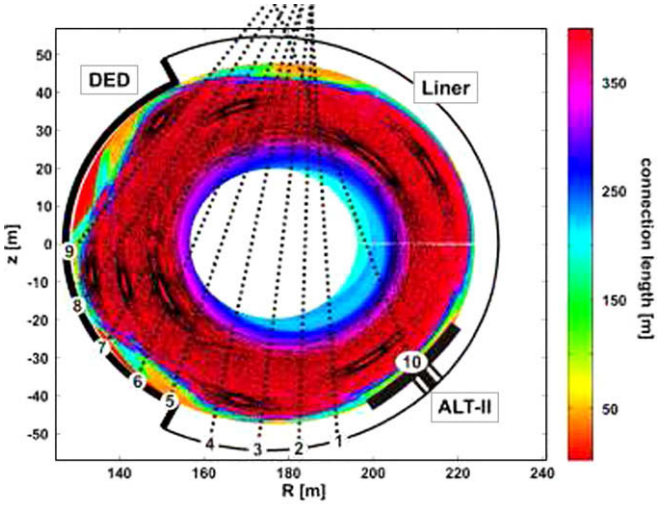

Fig. 1. Lines of sight of the UV carbon diagnostic superimposed to the magnetic field topology for the 3/1 basic mode (vacuum approximation).

Although other carbon lines are measured on TEXTOR along a single line-of-sight located at a different toroidal position by a

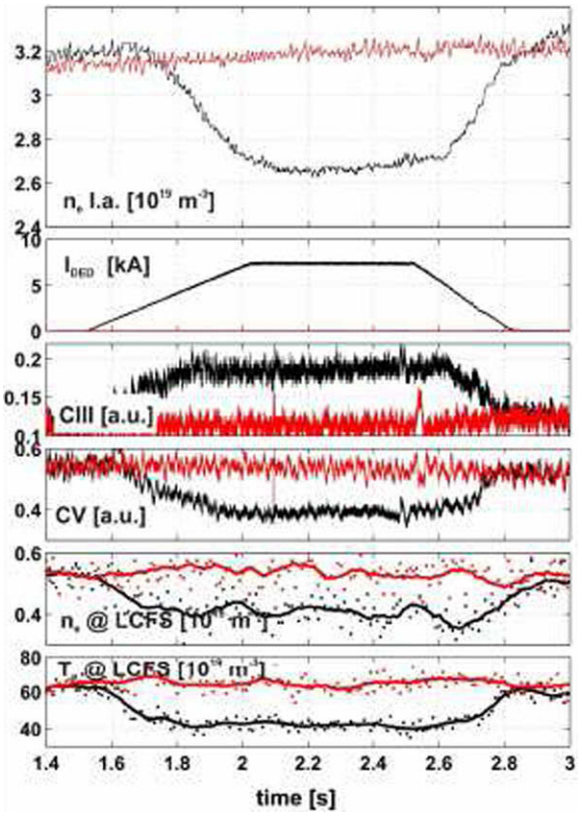

Fig. 2. From top: time traces of central line-average (l.a.) density, of I_{DED}, of CIII and CV signals for channel *N*. 4, of edge density and temperature for # 105783 (reference, without DED, in red) and # 105784 (with DED, in black), 6/2 basic mode . (For interpretation of the references to colour in this figure legend, the reader is referred to the web version of this article.) .

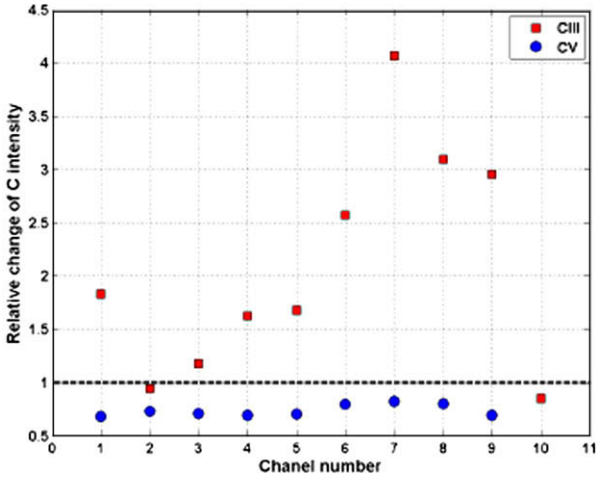

Fig. 3. Ratio of the carbon signals for # 105784 (with DED) and # 105783 (without DED), 6/2 basic mode.

vacuum spectrometer in the Vacuum-Ultra-Violet range, it is not always easy to relate these measurements to those of CIII and CV along the 10 channels, due to the 3-dimensional nature of the DED. However, the general tendency of these lines during DED operation is the increase in emission by carbon ions of low ionization potential and the reduction in emission by carbon ions of high ionization potential.

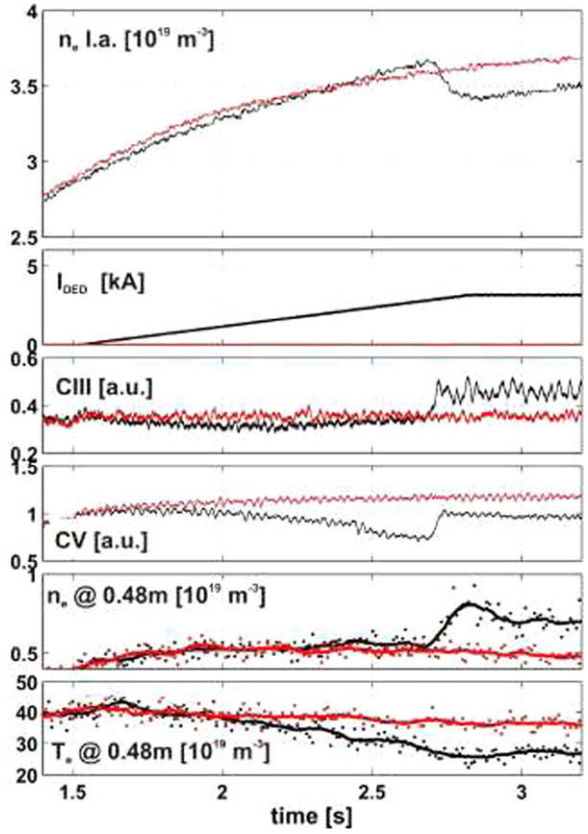

Fig. 4. From top: time traces of central line-average (l.a.) density, of I_{DED}, of CIII and CV signals for channel *N*. 3, and of edge density and temperature for # 105346 (reference, without DED, in red) and # 105348 (with DED, in black), 3/1 basic mode. (For interpretation of the references to colour in this figure legend, the reader is referred to the web version of this article.)

2.2. Basic mode 6/2

Due to the resonant character of the interaction between the perturbing field and the edge plasma [7], the best performances in terms of particle pump out are achieved for a value of the edge safety factor, $q(a)$, slightly above 3, both in 6/2 and in 3/1 DED basic modes. All the data presented in this paper refer to discharges with $q(a)$ in the range 3.3–3.6.

For DED 6/2 basic mode, in presence of full NBI-Cnt (about 1.5 MW), tearing modes are not triggered up to the maximum value of I_{DED} (= 7.5 kA, for 6/2 operation). At this value, the field line diffusion coefficient D_{fl} (which depends on the square of the perturbing field and on the local pitch angle of the equilibrium field) is of the order of 2×10^{-5} m^2/m and it reaches its maximum at about 5 cm inside the plasma (see Refs. [3,11]). Above a certain threshold in I_{DED} (see Ref. [7]), the central line-average electron density, nela, decreases smoothly with increasing I_{DED}, similarly to the behaviour of the CV line intensity (see Fig. 2). It can also be observed that the drop in the edge n_e and T_e occurs much earlier than that of the central line-average density and slightly earlier that the change in CIII and CV signals. In fact, the edge n_e and T_e are derived by local measurements while the central line-average electron density as well as the CIII and CV signals are integrals along chords. In Fig. 3 the ratios between the carbon line intensities with DED at full current and without DED are shown for all 10 channels. Here one sees that the decrease in the CV line intensity with DED is similar on all 9 channels and, on the average, it is of about 20%. The decrease of the C^{6+} ion concentration, measured by CXRS, is in the range 19 - 12% with respect to the reference dis-

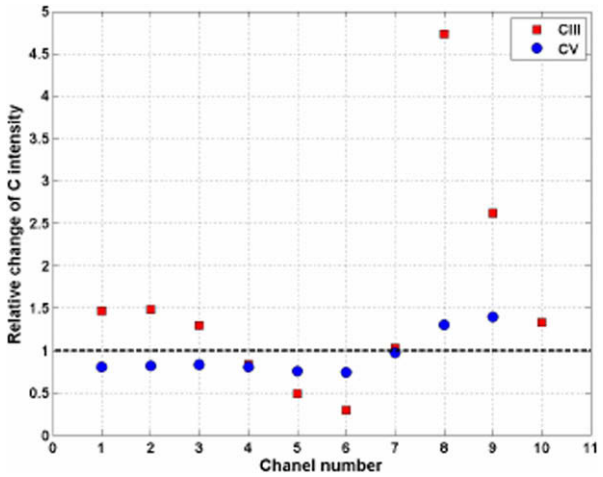

Fig. 5. Ratio of the carbon signals for # 105348 (with DED) and # 105346 (without DED), 3/1 basic mode.

charge (see Fig. 6 in Section 3) and it would imply, assuming carbon as the dominant impurity, a reduction of Z_{eff} from 2.1 to 1.9 at t = 2.2 s, in spite of the reduction in the central line-average density. The behaviour of the CIII line is more complex, since CIII radiation is emitted near the carbon source which is strongly asymmetrical both in poloidal and toroidal directions as a consequence of the 3-dimensional nature of DED and of its interaction with the wall. For example, for the configuration of the discharges used in Fig. 2 the CIII line increases up to a factor of 4 on the channels pointing at the divertor tiles (*N*.5–9) while it increases or decreases slightly on the other channels. (To account for the difference in the response between channels 1 and 2, one should consider that even in the presence of DED the graphite ALT-II toroidal limiter in the LFS remains a significant source of carbon and, by consequence, the intensity of CIII line may also be related to local effects caused by the limiter edge. Moreover changes of the local density may contribute to the different response of the CIII lines as well as 3-D effects.) This is in good agreement with CIII line measurements made in the visible by a camera located at a different toroidal sector, which show a significant increase of the CIII light both on the HFS and LFS. Unfortunately, a quantitative comparison of the spectroscopic data with the bolometric data is not possible for these discharges since one out of the four cameras was not operational during the experimental campaign considered. The edge electron density profile-measured by the He-beam diagnostic on the LFS-decreases generally by about 20%, similarly to the average density. Although the central electron temperature remains unchanged during DED operation, the edge temperature shows a pronounced decrease, from about 60 eV to about 45 eV at $r = a$ = 0.46 m for the shot shown in Fig. 2.

2.3. Basic mode 3/1

Differently from the 6/2 basic mode, in 3/1 basic mode the current in the DED coils cannot be raised to its maximum level ($I_{DED,max}$ = 3.75 kA) without triggering the 2/1 tearing mode, due to the larger penetration of the perturbing field. Therefore, in all the discharges examined in this paper I_{DED} is limited to 3.2 kA. A second difference consists in the stepwise character of the effects of DED on transport with increasing I_{DED}, which can be clearly seen when I_{DED} is ramped up sufficiently slowly, see Fig. 4. In fact, increasing I_{DED} up to about 2.5 kA the average density may (in some cases) decrease smoothly with respect to the reference without DED or it may remain nearly unchanged (as in the example in Fig. 4), depending on the level of saturation of the wall, while the CV line intensity decreases significantly in many channels. One can notice a small increase in the electron density (with respect to the reference discharge) just before the onset of the PO as for the 6/2 basic mode, consistent with a transient improvement of the main particle confinement prior to PO (see Ref. [7] for a detailed description), while some effects of the field stochastization are seen in the decrease of both the CV line (de-contamination) and the edge temperature. The constancy of the CIII signal in this phase indicates that the carbon source is practically unaffected on this channel (see below). One should also note that, in contrast with the discharges of Fig. 2 (6/2 basic mode), due to bad wall condition during the 3/1 basic mode campaign, the electron density could not be kept constant also during the reference discharges, leading to the increase of the electron density with time. For $I_{DED} > 2.5$ kA an abrupt drop in the average density (in the range 10–20%) is accompanied by an abrupt *increase* of both CIII and CV signals. The increase of CIII and CV signals (the CV signal does not, however, recover the value before DED) is correlated with a simultaneous increase of the edge density (up to 30%), while the edge temperature

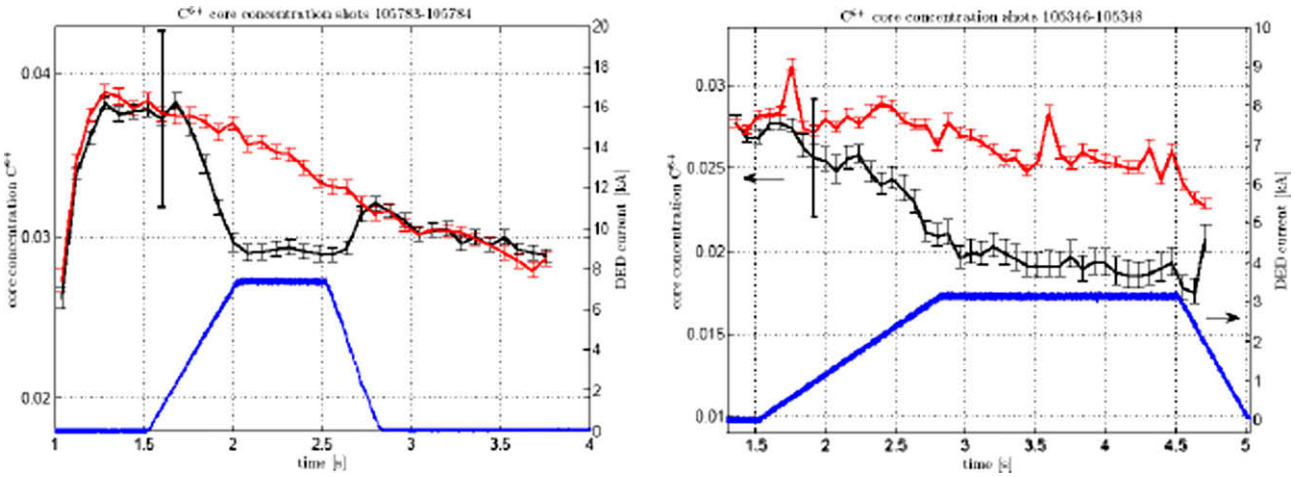

Fig. 6. Time traces of the C^{6+} ion concentration and of I_{DED} for # 105783 (reference, without DED, in red) and # 105784 (with DED, in black), 6/2 basic mode (left) and for # 105346 (reference, without DED, in red) and # 105348 (with DED, in black), 3/1 basic mode (right). (For interpretation of the references to colour in this figure legend, the reader is referred to the web version of this article.)

decreases, as for the 6/2 basic mode. In Fig. 5, the ratios of line intensities between the discharge with I_{DED} = 3.2 kA and the reference without DED is shown for the 10 channels. The CIII ratios, which reflect the change in the carbon source with DED, show a peak (channels 8–9) and a depression (channels 5–6) which correspond to the strike points and to the private region, respectively. One can also observe that the structure in CIII ratios as shown in Fig. 3 for the 6/2 basic mode is more complex than that of Fig. 5, as a consequence of the higher poloidal mode numbers of the 6/2 basic mode. With respect to the CV ratios in Fig. 5, the CV ratios decrease everywhere with the exception of those channels pointing at the strike points (channels 8–9) where the CIII ratios increase considerably. The CIII data are in quantitative agreement with visible measurements of the CIII line, as for the 6/2 basic mode, while CV data have to be correlated with the CXRS diagnostic which shows a decrease of the carbon concentration in the plasma center (see Section 3).

3. Discussion

In this work, for 6/2 basic mode the main particle confinement time τ_p, estimated using the intensity of the D_α line and the level of the electron density [7], shows a reduction in τ_p proportional to I_{DED} in agreement with a diffusion dominated analytical model [13]. Indeed, in the frame of the present study, changes in the effective radial transport caused by classical parallel diffusivity along the stochastic field lines account for the changes in particle (and impurity) transport. Even though modifications in anomalous transport have been observed in TEXTOR during DED operation [14], they are not considered in the present discussion. For 6/2 basic mode τ_p decreases by about 20% with respect to the reference without DED as does the electron density, while for 3/1 basic mode with $I_{DED} < 2.5$ kA the decrease of τ_p is limited to a few percent, with minor change in the average electron density. Considering that the level of stochastization is comparable for the above considered two conditions (field line diffusion, D_{FL}, of the order of $2–3 \times 10^{-5}$ m^2/m) and that for 3/1 basic mode with $I_{DED} < 2.5$ kA the decrease in carbon concentration is about 16% with respect to the reference discharge (see Fig. 6), these data indicate a similar effect on carbon transport for 3/1 basic mode. For 3/1 basic mode at I_{DED} = 2.5 kA the width of a 3/1 tearing island becomes such (6 cm, according to ECE measurements) that the island connects to the wall [7] with a related local increase in the edge electron density. The sudden drop in the average density (see Fig. 4) and the increase in the edge density at I_{DED} = 2.5 kA are related, respectively, to a significant drop in τ_p (20%) and to the increase in the CIII and CV signals. Consistently, CXRS measurements show a decrease in the C^{6+} ion concentration down to a further 10% with increasing I_{DED} above 2.5 kA Fig. 6.

4. Conclusion

Although the 3-dimensional nature of the action of DED limits the possibility of quantitative conclusion on the basis of local measurements at the plasma edge (for example, it is difficult to give a number for the carbon screening defined by the ratio of the total carbon flux and the carbon density in the plasma core), the full body of the experimental data allows drawing the following conclusion.

Operation in PO regime and in 3/1 basic mode for $I_{DED} < 2.5$ kA causes de-contamination of highly charged carbon ions in the stochastic layer as a consequence of the enhanced effective radial diffusivity of the main ions in the stochastic layer. According to an analytical model [15], the main ions drag out selectively high Z impurities via frictional forces, which increase with the square of charge. That is the reason why to the generally observed increase in carbon flux with DED, it corresponds a moderate decrease in the density of the C^{4+} ions (leading normally to the constancy of their concentration, considering the reduction of the edge density) and also a more relevant decrease of the C^{6+} ions density, which causes a significant reduction in the concentration of fully stripped carbon ions. A similar effect on carbon transport is seen when-in 3/1 basic mode at $I_{DED} > 2.5$ kA-the 3/1 island connects to the wall, even though we do not have yet a clear understanding of the mechanism responsible for the related local increase of the edge density. On the other hand, impurity transport in the plasma center, where the effects of stochastization vanishes, remains unaffected by the application of RMP, as shown by experiments on TEXTOR.

References

[1] T. Evans et al., Nature Phys. 2 (2006) 419.
[2] Y. Liang et al., Phys. Rev. Lett. 98 (2007) 265004.
[3] O. Schmitz et al., Nucl. Fus. 48 (2008) 024009.
[4] S.S. Abdullaev et al., Phys. Plasmas 6 (1999) 153.
[5] K.H. Finken et al., Nucl. Fus. 38 (1998) 515.
[6] M. Lehnen et al., Plasma Phys. Control. Fus., 47 (2005) B237.
[7] O. Schmitz et al., J. Nucl. Mater. 390–391 (2009) 330.
[8] G. Telesca et al., J. Nucl. Mater. 337–339 (2005) 361.
[9] G. Telesca et al., in: Proceedings of the Thirty Third EPS Conference on Plasma Physics, vol. 30I, Rome, Italy, 19–23 June 2006, CA, P2.157.
[10] H.R. Koslowki et al., Plasma Phys. Control. Fus., 48 (2006) B53.
[11] M. Jakubowski et al., Nucl. Fus. 44 (2004) S1.
[12] O. Schmitz et al., Plasma Phys. Control. Fus., 50 (2008) 115004.
[13] M.Z. Tokar et al., Phys. Rev. Lett. 98 (2007) 095001.
[14] Y. Xu et al., Phys. Rev. Lett. 97 (2005) 165003.
[15] M.Z. Tokar et al., Plasma Phys. Control. Fus., 39 (1997) 569.